

Finite Element Analysis of Thermoelastic Damping in Contour-Mode Vibrations of Micro- and Nanoscale Ring, Disk, and Elliptical Plate Resonators

Yun-Bo Yi

Department of Mechanical and Materials
Engineering,
University of Denver,
Denver, CO 80208
e-mail: yyi2@du.edu

Thermoelastic damping in contour-mode in-plane vibrations of rings, disks, and elliptical plates is investigated on various size scales, using a reduced finite element formulation. The Fourier scheme is applied to the axisymmetric geometries including circular rings and disks, and is found to be remarkably efficient in searching solutions. The numerical accuracy is further improved by the implementation of quadratic interpolation functions. The computational results are validated by comparing with the commercial software packages as well as the existing analytical solutions in literature. For resonators of elliptical shapes, the dominant frequency has a weak dependence on the geometric aspect ratio γ , whereas the effect of γ on the quality factor (Q value) is much stronger and the peak Q value of the leading mode consistently occurs in the vicinity of $\gamma=1.42$.
[DOI: 10.1115/1.4001506]

1 Introduction

Over the past decade thermoelastic damping has been an active research area in design, optimization, fabrication, and testing of microelectromechanical systems (MEMS) and nanoelectromechanical systems (NEMs) against internal energy dissipation [1,2]. Although the mechanism of thermoelastic damping was explained long time ago by Zener [3], the modern application of the theory to micro- and nanoscale resonators should be attributed to Lifshitz and Roukes [4] who successfully predicted the thermoelastic damping dissipation in simple beam resonators. Recent researchers extended the method to other related problems, both analytically [5] and numerically [6]. Meanwhile a number of practical techniques were suggested for minimizing the thermoelastic damping [7]. It has been noticed that Wong et al. [8] studied the resonance of MEMS gyros, which was the first time an axisymmetric system was analyzed. Later, Sun and Tohmyoh [9] investigated the circular plate resonators, but their work was restricted to out-of-plane vibration modes. A more comprehensive study on disk resonators was performed by Hao [10] who presented some interesting results on the contour-mode vibrations of circular thin-plate resonators. The analytical methods and classical theories of elasticity were applied to derive the generation rate of thermal energy per cycle of vibration, from which the quality factor was successfully determined. In Hao's work, although the methodology itself was based on a sound groundwork, some of the key results on the quality factor have been found about an order of magnitude higher than those predicted by the commercial codes and other methods, and therefore are somehow misleading. A revisit of the problem using a more systematic approach is therefore necessary.

In addition, the analytical approach is restricted to beams or axisymmetric structures such as circular disks with homogeneous boundary conditions. Recent advances in the NEMS and MEMS technologies, however, enable thin-plate resonators operating in

their elliptical vibration modes [11,12]. Future extension of the technology may directly involve the fabrication of elliptical plate resonators. A comparison between the performances of circular disks and noncircular plates will become important for optimal designs. The finite element method is a suitable tool for this purpose. In general, the advantage of the finite element method over the analytical approach lies that there is no restriction on the complexity of device geometries, boundary conditions, and the loading methods. For example, more complex geometries containing vent sections and thin film deposition can be handled in the same way. These sections and thin layers can prevent the heat flow across the device or minimize the surface tractions, and therefore it is expected that they will reduce the thermoelastic energy dissipation.

Employing a commercial software package such as COMSOL [13] is an obvious solution. However, in these commercial codes, the solution algorithm is typically based on the general-purpose complex eigenvalue solver that involves an iteration scheme, and therefore an initial guess of the solution is often required as an input. In fact, for this particular application, there exists a more efficient method, which was already elaborated in the author's prior works [14,15]. These works were focused on the out-of-plane flexural-mode vibrations; however, the analytical approximations showed that the in-plane contour-mode vibrations have much different key characteristics. It is therefore natural to extend the method to the contour-mode vibrations. In addition, the previous work showed that using linear finite elements often gave rise to unsatisfactory numerical accuracy and efficiency [16]. In the current research, we aim to establish a method based on the non-linear interpolation functions to achieve a better numerical performance. We will start from simple beam systems then extend the method to rings, disks, and elliptical plates.

2 Method

2.1 Governing Differential Equations. A key design parameter of a resonator is the quality factor or Q value (Q -factor). It is crucial that the resonator vibrates at the desired frequency and that it requires as little energy as possible to maintain its vibration at that frequency. The Q value is essentially a measure of the sharp-

Contributed by the Technical Committee on Vibration and Sound of ASME for publication in the JOURNAL OF VIBRATION AND ACOUSTICS. Manuscript received June 16, 2009; final manuscript received March 25, 2010; published online July 15, 2010. Assoc. Editor: Cheng-Kuo Sung.

ness of the vibrational spectrum's peak [17]. To define this key parameter, we need to compute or measure the energy loss per cycle ΔW , and compare it to the total stored kinetic energy W ; i.e.,

$$Q = \frac{2\pi W}{\Delta W} = \frac{\omega}{2\delta} = \frac{\omega}{\Delta\omega} \quad (1)$$

where ω is the natural frequency, δ is the exponential damping factor (namely, the decaying rate of oscillation in time δt), and $\Delta\omega$ is the half power width of the spectrum.

In the theory of thermoelasticity, the relation between the mechanical stress $\boldsymbol{\sigma}$ and strain $\boldsymbol{\varepsilon}$ is given by

$$\boldsymbol{\sigma} = D(\boldsymbol{\varepsilon} - \boldsymbol{\varepsilon}_t) \quad (2)$$

where $\boldsymbol{\varepsilon}$ is the elastic strain without thermal effects and $\boldsymbol{\varepsilon}_t$ is the thermal strain. D is the 6×6 elasticity matrix, and all stresses and strains are denoted with second-order tensors consisting of x , y , and z normal components followed by the x - y , y - z , and x - z shear components.

In the theory of dynamics and vibration, the equation of motion is established on the basis of the following force equilibrium:

$$\rho \frac{\partial^2 \mathbf{u}}{\partial t^2} = \nabla \cdot \boldsymbol{\sigma} \quad (3)$$

where ρ is the material density, \mathbf{u} is the displacement vector, and $\boldsymbol{\sigma}$ is the stress tensor.

The corresponding thermal problem is governed by the heat diffusion equation as follows:

$$\rho c_p \frac{\partial T}{\partial t} - \nabla \cdot (k \nabla T) = \dot{q} \quad (4)$$

where c_p is the specific heat capacity, k is the thermal conductivity, and \dot{q} is the heat source—namely, the heat generation rate per unit volume. In thermoelastic damping, the heat source comes from the thermoelastic heating, which for an isotropic material has the explicit form

$$\dot{q} = - \frac{E\alpha T_0}{(1-2\nu)} \frac{\partial \bar{\varepsilon}}{\partial t} \quad (5)$$

where E is Young's modulus, α is the coefficient of thermal expansion, ν is Poisson's ratio, T_0 is the initial temperature, and $\bar{\varepsilon}$ is the dilatation strain defined by

$$\bar{\varepsilon} = \varepsilon_x + \varepsilon_y + \varepsilon_z = \nabla \cdot \mathbf{u} \quad (6)$$

For the two-dimensional plane stress condition, the stress component σ_z vanishes. From Eq. (2) it follows

$$\sigma_z = \frac{E}{(1+\nu)(1-2\nu)} [\nu \varepsilon_x + \nu \varepsilon_y + (1-\nu)\varepsilon_z - \alpha(T-T_0)(1+\nu)] = 0 \quad (7)$$

Therefore,

$$\varepsilon_z = - \frac{\nu}{1-\nu} (\varepsilon_x + \varepsilon_y) + \frac{1+\nu}{1-\nu} \alpha(T-T_0) \quad (8)$$

Substituting this into Eq. (5) yields

$$\dot{q} = - \frac{E\alpha T_0}{(1-2\nu)(1-\nu)} \left[(1-2\nu) \frac{\partial(\varepsilon_x + \varepsilon_y)}{\partial t} + (1+\nu)\alpha \frac{\partial T}{\partial t} \right] \quad (9)$$

2.2 Finite Element Formulations. We assume an exponential perturbation solution [18,19] of the form

$$\begin{aligned} T - T_0 &= \Re\{e^{bt}\boldsymbol{\Theta}\} \\ \mathbf{u} &= \Re\{e^{bt}\mathbf{U}\} \\ \mathbf{u}' &= \Re\{e^{bt}\mathbf{V}\} \end{aligned} \quad (10)$$

where \Re represents the real part of a complex number, b is the

complex exponential growth rate, and \mathbf{u}' is the velocity vector.

By discretization, the heat diffusion equation can be written in the matrix form as

$$(\mathbf{K} + b\mathbf{H})\boldsymbol{\Theta} + b\mathbf{F}\mathbf{U} = \mathbf{0} \quad (11)$$

where \mathbf{K} , \mathbf{H} , and \mathbf{F} are coefficient matrices; $\boldsymbol{\Theta}$ is the nodal temperature; and \mathbf{U} is the nodal displacement. In the above equation, the dilatation strain is related to the nodal displacement via the following consideration:

$$\boldsymbol{\varepsilon} = \mathbf{B}\mathbf{U} \quad (12)$$

where \mathbf{B} is a coefficient matrix determined by the element shape and the interpolation function. Accordingly the matrix equation of motion is given by

$$\mathbf{L}\mathbf{U} - \mathbf{G}\boldsymbol{\Theta} + b\mathbf{M}\mathbf{V} = \mathbf{0} \quad (13)$$

where \mathbf{L} , \mathbf{G} , and \mathbf{M} are coefficient matrices, and \mathbf{V} is the nodal velocity.

In addition to the above matrix equations, there exists an intrinsic relationship between the displacement and velocity perturbations as follows:

$$\mathbf{V} = b\mathbf{U} \quad (14)$$

This is due to the fact that the velocity is the first derivative of the displacement.

2.3 Eigenvalue Equation. Combining Eqs. (11), (13), and (14) yields

$$\begin{bmatrix} -\mathbf{K} & 0 & 0 \\ \mathbf{G} & -\mathbf{L} & 0 \\ 0 & 0 & \mathbf{I} \end{bmatrix} \begin{Bmatrix} \boldsymbol{\Theta} \\ \mathbf{U} \\ \mathbf{V} \end{Bmatrix} = b \begin{bmatrix} \mathbf{H} & \mathbf{F} & 0 \\ 0 & 0 & \mathbf{M} \\ 0 & \mathbf{I} & 0 \end{bmatrix} \begin{Bmatrix} \boldsymbol{\Theta} \\ \mathbf{U} \\ \mathbf{V} \end{Bmatrix} \quad (15)$$

where \mathbf{I} is an identity matrix. This is a standard eigenvalue equation. The eigenvalue in the equation is the growth rate b and the eigenvector is $\{\boldsymbol{\Theta}, \mathbf{U}, \mathbf{V}\}^T$. It is important to note that by formulating the velocity field as a perturbation component independent of displacement, the originally quadratic equation is now reduced to a first-order eigenvalue problem; therefore the computational effort has substantially been reduced.

In the above eigenvalue formulation, the quality factor of the vibration can be related to the eigenvalue b as follows:

$$Q = \left| \frac{\Im(b)}{2\Re(b)} \right| \quad (16)$$

where $\Re(b)$ and $\Im(b)$ represent the real part and the imaginary part of b , respectively. Since the coefficient matrices in Eqs. (11)–(13) were already presented in the prior work [15], the detailed derivations are omitted here for brevity. The entire finite element algorithm has been incorporated in a customized MATLAB code bundle that integrates the preprocessing procedure, eigenvalue solver, and postprocessing procedure.

2.4 Axisymmetric Problems. For a three-dimensional annular ring or disk problem, the formulation of the eigenvalue equation is essentially the same as above. However, the plane stress assumption will be removed and all three degrees of freedom will be taken into consideration. The finite element discretization is performed on the cross sectional domain only; therefore, it substantially reduces the computational effort. The solution to the problem is a function of the prescribed Fourier number (namely, the number of the circumferential waves m); therefore this method can be called as *the Fourier method*. To simulate the in-plane contour motion, the boundary is constrained on the bottom surface of the ring/disk along the axial direction and hence only the radial motion is allowed for the bottom nodes. The other surface is traction-free, thus equivalent to the plane stress situation in the two-dimensional model. Again, the detailed derivations of the relevant elemental matrices were already presented in the author's prior work [14], and therefore they are omitted here for brevity.

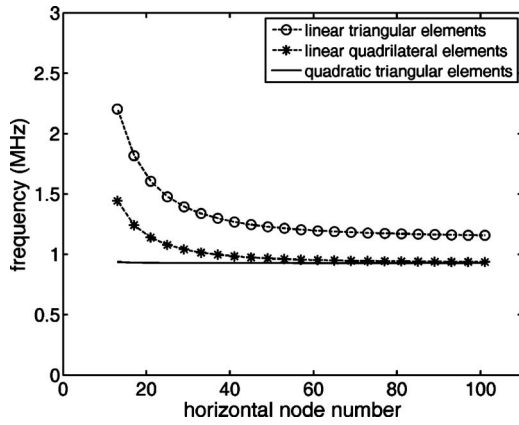


Fig. 1 Convergence test for the resonant frequency of flexural-mode vibrations of simply supported beams using both linear and nonlinear elements

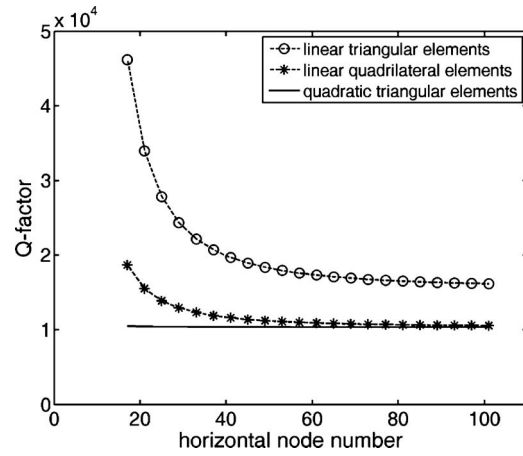


Fig. 2 Convergence test for the quality factor of flexural-mode vibrations of simply supported beams using both linear and nonlinear elements

2.5 Construction of Quadratic Finite Elements. For the rectangular elements used in the analysis, we assume the nine-node nonlinear plain stress element type with the quadratic interpolation functions [20] defined by

$$\begin{aligned}
 \psi_1 &= (s^2 - s)(\eta^2 - \eta)/4 \\
 \psi_2 &= (1 - s^2)(\eta^2 - \eta)/2 \\
 \psi_3 &= (s^2 + s)(\eta^2 - \eta)/4 \\
 \psi_4 &= (s^2 - s)(1 - \eta^2)/2 \\
 \psi_5 &= (1 - s^2)(1 - \eta^2) \\
 \psi_6 &= (s^2 + s)(1 - \eta)/2 \\
 \psi_7 &= (s^2 - s)(\eta^2 + \eta)/4 \\
 \psi_8 &= (1 - s^2)(\eta^2 + \eta)/2 \\
 \psi_9 &= (s^2 + s)(\eta^2 + \eta)/4
 \end{aligned} \tag{17}$$

where s and η are the local coordinates inside the rectangle. For triangular elements, we assume the six-node nonlinear element type with the quadratic interpolation functions defined by

$$\begin{aligned}
 \psi_1 &= L_1(2L_1 - 1) \\
 \psi_2 &= 4L_1L_2 \\
 \psi_3 &= L_2(2L_2 - 1) \\
 \psi_4 &= 4L_2L_3 \\
 \psi_5 &= L_3(2L_3 - 1) \\
 \psi_6 &= 4L_1L_3
 \end{aligned} \tag{18}$$

where L_i ($i=1,2,3$) are the area coordinates of a triangle.

3 Results and Discussions

3.1 Validation of the Method for Beams. Since the thermoelastic damping solutions for the flexural-mode vibrations of beams were widely reported in literature, it is natural to use the existing beam solutions to validate the model developed in the current work as the first step. As opposed to the linear elements used in the prior research [15], quadratic finite elements have been implemented here for the first time.

Shown in Figs. 1 and 2 are the convergence tests for the resonant frequency and Q value using both linear and nonlinear elements in the flexural-mode vibrations of simply supported beams. Polysilicon properties listed in Table 1 were assumed. The beam length is 200 μm and its thickness is 10 μm . Poisson's ratio ν was set to zero so that the results can be compared to the LR solution (i.e., Lifshitz and Roukes' analytical solution [4]). Clearly the linear triangular elements converge very slowly. Using 101 nodes along the length, there is a 24.7% deviation for the frequency and 55.7% deviation for the Q value. The linear quadrilateral elements give a better solution: For a beam of 101 nodes along the length, the results are quite close to the exact solution. However, a total node number of less than 50 may lead to a much appreciable numerical error. In contrast, the quadratic elements result in a much faster convergence speed. In both Figs. 1 and 2, the curves for quadratic elements almost remain horizontal throughout the entire range of the node number. When the node number is greater than 30, there is virtually no difference between the two solutions. In fact, with only 13 nodes along the beam length, the result is different from the LR solution by less than 1% for the frequency and less than 2% for the Q value. As a consequence it has proved to be much more efficient using the quadratic elements than the linear elements in the current model.

To further validate the approach, the dynamic responses of a beam have been determined as functions of the beam thickness and compared with the LR solution. In Figs. 3 and 4, the parameter ξ is defined by

$$\xi = h \sqrt{\frac{\omega_0 \rho C_p}{2k}} \tag{19}$$

where for a simply supported beam, the first undamped natural frequency ω_0 is

Table 1 Material properties of polysilicon

Young's modulus (Pa)	1.57×10^{11}
Poisson's ratio	0.22
Thermal expansion coefficient (K^{-1})	2.6×10^{-6}
Thermal conductivity ($\text{W m}^{-1} \text{K}^{-1}$)	90
Specific heat ($\text{m}^2 \text{s}^{-1}$)	700
Density (kg/m^3)	2330
Temperature (K)	300

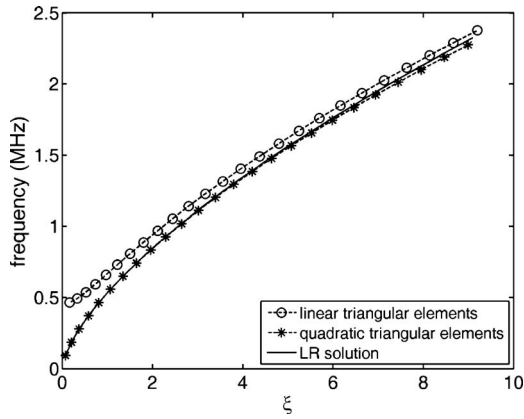


Fig. 3 Comparison of the resonant frequency (as a function of beam thickness) between the finite element model and the *LR* solution for the flexural-mode vibrations of simply supported beams

$$\omega_0 = 2.8491 \frac{h}{L^2} \sqrt{\frac{E}{\rho}} \quad (20)$$

in which h is the beam thickness and L is the beam length. Both linear and quadratic triangular elements have been compared in the figure. The node number in the length was maintained as 51 for both element types involved. From Fig. 3, clearly the results obtained from the quadratic elements are almost identical to the *LR* solution, except for large ξ , or large beam thickness, where the beam theory (namely, the theory based on the assumption that the plane sections remain plane) does not rigorously apply. In contrast, the linear elements yield much poorer solution, especially for small beam thicknesses. Figure 4 tells the same story; i.e., the quadratic elements result in a much better solution than the linear elements for predicting the Q value. For example, at the lowest point on the curve, which is located at $\xi=2.2246$, the Q value predicted by the linear elements is approximately 31.7% higher than the *LR* solution or the result predicted by the quadratic elements.

3.2 Circular Disks. After the methodology was validated for flexural-mode beam resonators, it was then implemented in the contour-mode vibrations of circular disks. For consistency the same polysilicon material properties have been assumed here. The computational results were first compared to the multiphysics commercial package COMSOL. In the COMSOL model, both a full

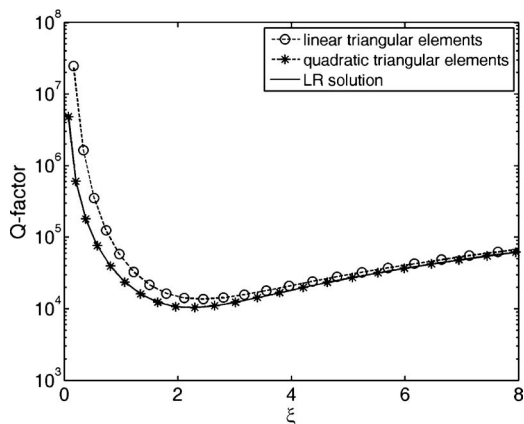


Fig. 4 Comparison of the quality factor between the finite element model and the *LR* solution for the flexural-mode vibrations of simply supported beams

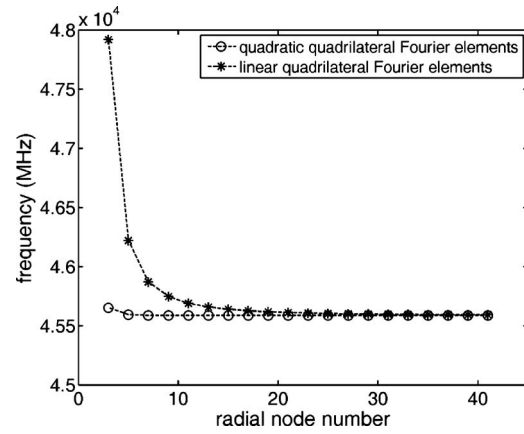


Fig. 5 Convergence test for the resonant frequency of the contour-mode vibrations of circular disks using both linear and nonlinear Fourier elements ($r=43$ nm, $m=2$)

disk model and a quarter disk model were constructed to compute the resonant frequency and Q value. The quarter model was subjected to symmetrical boundary conditions on the two straight edges for improving the computational efficiency. The disk radius was set to 43 nm and m was set to 2, which were consistent with the parameters used in Hao's paper [10]. Both COMSOL models yielded the frequency 45.59 GHz and the Q value of 3.956×10^5 . In Figs. 5 and 6, the predicted results are shown by using the linear and quadratic Fourier elements constructed on the cross sectional plane of the disk. The results are expressed as functions of the radial node number. The node number in the thickness direction was set to three so that there were two elements through the thickness in the linear model and one element in the corresponding nonlinear model. For the computed frequency, both linear Fourier elements and quadratic Fourier elements converge to 45.59 GHz. Apparently, in view of the convergence speed, the latter element type performs much better than the former one. With only three nodes along the radius, the quadratic Fourier model is capable of yielding a result very close to the exact solution. In more general, ten radial elements are sufficient for a satisfactory numerical accuracy. For the Q value result as shown in Fig. 6 we can draw the same conclusion: The predicted Q value converges to the COMSOL solution for both types of elements but the quadratic model converges much faster than the linear model. On the other hand, it implies that Hao's analytical solution on the Q value (1.605×10^6) is about an order of magnitude higher than

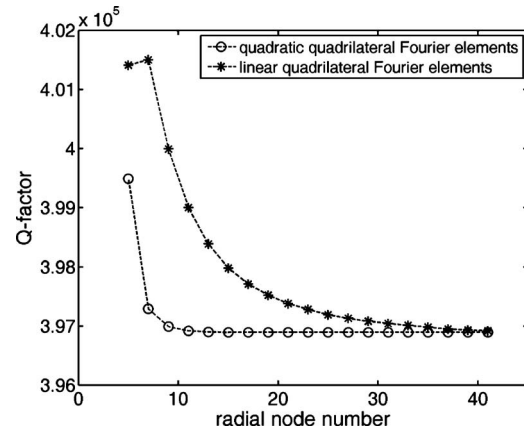


Fig. 6 Convergence test for the quality factor of the contour-mode vibrations of circular disks using both linear and nonlinear Fourier elements ($r=43$ nm, $m=2$)

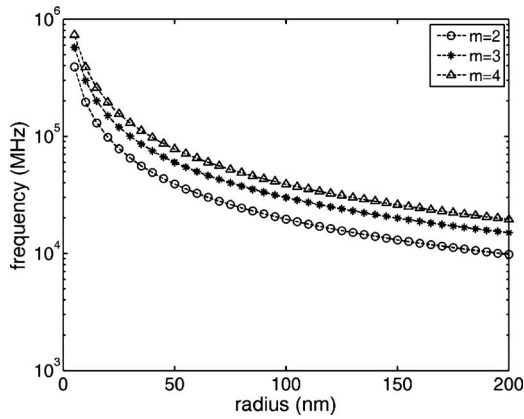


Fig. 7 Frequency of the leading mode of contour-mode vibration of circular disks as a function of disk radius

the correct solution, and therefore is erroneous for some unknown reasons.

In the next step the axisymmetric Fourier model has been used to study the effect of the disk radius, and the results are presented in Figs. 7 and 8. The first three resonant modes corresponding to $m=2, 3$, and 4 are investigated for comparison. In Fig. 7 we can see that the frequencies monotonically decrease with the radius. In Fig. 8, the minimum Q values on the curves are located in the vicinity of $r=43$ nm, 53 nm, and 65 nm for $m=2, 3$, and 4, respectively. These locations agree with Hao's results very well although the corresponding Q values are consistently about an order of magnitude lower than Hao's results. A closer inspection on the curves also reveals that there are crossovers among the curves for small radii. For example, the Q value for $m=4$ is higher than that for $m=3$ when $r=5$ nm. This type of crossover is not seen in the figures presented in Hao's paper.

3.3 Circular Rings. The same model was also used to compute the results for the contour-mode vibrations of circular rings instead of disks. First, the ring model was compared to the results obtained by Wong et al. [8]. Their approach was based on the analytical method and the fundamental beam theory was employed; thus Poisson's ratio was absent in their formulations. By using the silicon properties assumed in their paper and setting $\nu=0$, the ring model based on the Fourier finite element scheme has been established and the results were found very close to Wong's solutions (as shown in Table 2), therefore further validate the Fourier model developed in the current work.

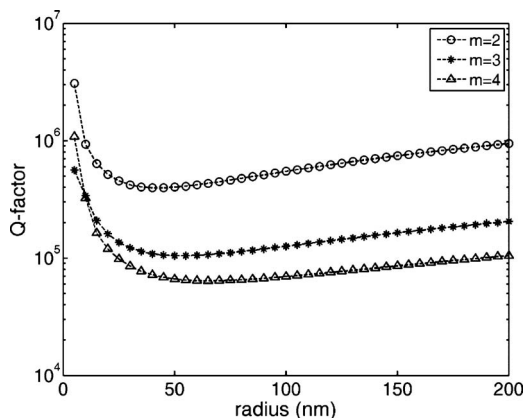


Fig. 8 Quality factor of the leading mode of contour-mode vibration of circular disks as a function of disk radius

Table 2 Comparison of quality factor for contour-mode vibration of silicon rings when $m=2$

Radius (mm)	Radial thickness (μm)	Q value (Wong's solution)	Q value (current work)
5	160	1.026×10^4	1.025×10^4
3	120	1.075×10^4	1.074×10^4
3	80	1.365×10^4	1.364×10^4
2	60	1.415×10^4	1.414×10^4
2	40	4.137×10^4	4.133×10^4

A parametric study was then performed based on the geometric data used in Hao's model. The outer radius of the ring was fixed in all cases and the inner radius varied between the outer radius and zero value. The results were found to be dependent on the ratio of the inner and outer radii R_i/R_o . From Figs. 9 and 10 it is seen that while the frequency monotonically decreases with R_i/R_o , there is a lowest point of the Q value. For example, when $R_o=43$ nm and $m=2$, the minimum value is located in the vicinity of $R_i/R_o=0.35$.

3.4 Elliptical Thin Plates. Finally, the analysis was extended to polysilicon elliptical thin plates, in which the Fourier scheme is no longer applicable because of the presence of the geometric asymmetry. A quarter disk model with symmetrical boundary conditions was developed with the element type being plane stress quadratic triangles. To validate the approach, the plane stress quarter model was first tested for a circular disk of radius 43 nm

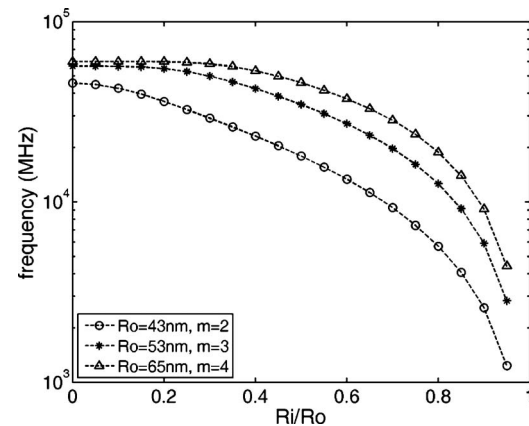


Fig. 9 Frequency of the contour-mode vibration of circular ring as a function of R_i/R_o

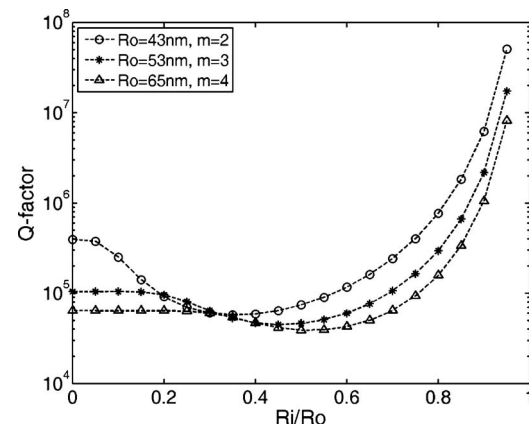


Fig. 10 Quality factor of the contour-mode vibration of circular ring as a function of R_i/R_o

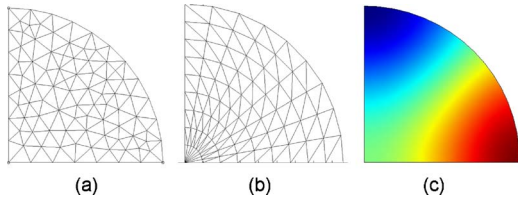


Fig. 11 Two-dimensional plane stress finite element model for the contour-mode vibration of circular plates: (a) free mesh, (b) lattice mesh, and (c) the dominant eigenmode

and compared to the validated Fourier model. Shown in Fig. 11 is the dominant eigenmode pattern along with the triangular finite element meshes. The model was discretized into either a free mesh using Delaunay tessellation or a regular mesh involving repeated patterns in both radial and tangential directions. The two meshes yielded almost identical results for the frequency (45.59 GHz) and the Q value (3.956×10^5). These values agree very well with the results obtained from the Fourier model and the COMSOL model. For elliptical plates, the key parameter is the aspect ratio (γ) of the geometry, which is defined by the ratio of the major axis length to the minor axis length. While varying the aspect ratio, the area was maintained the same so that the results were comparable to those of circular disks. From Fig. 12 it is seen that the frequency response has a mild dependence on the aspect ratio. For example, when the mean radius is 20 nm, the resonant frequency changes from 98.3 GHz to 70.4 GHz when γ is varied between 1 and 3 . The maximum variation in the frequency is less than 30% . The Q value, however, has a much stronger dependence on the aspect ratio, which can be seen in Fig. 13. The peak Q value of the leading mode can be 20 times higher than the minimum value on the curve. On the other hand, both frequency and maximum Q value decrease with the mean plate radius. Another interesting finding is that the peak value consistently occurs at $\gamma=1.42$ regardless of the mean radius. The drastic change in the dominant Q value could be closely related to the migration of the leading mode pattern. Figure 14 displays the temperature distributions in different eigenmode patterns corresponding to $\gamma=1.42$, whose frequencies and Q values are tabulated in Table 3. In some modes, the oscillation in the temperature field occurs along the major axis; in some modes, however, the variation is along the minor axis; in the remaining modes, the variation is along both directions. It is seen from Table 3 that the neighboring modes have close frequencies but the leading mode has a significantly higher Q value compared to other modes. When the aspect ratio changes, an originally higher-order mode pattern will alter its frequency

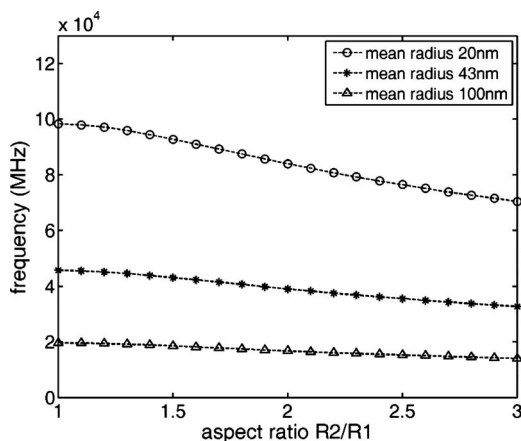


Fig. 12 Frequency as a function of geometric aspect ratio in the contour-mode vibration of elliptical plate resonators

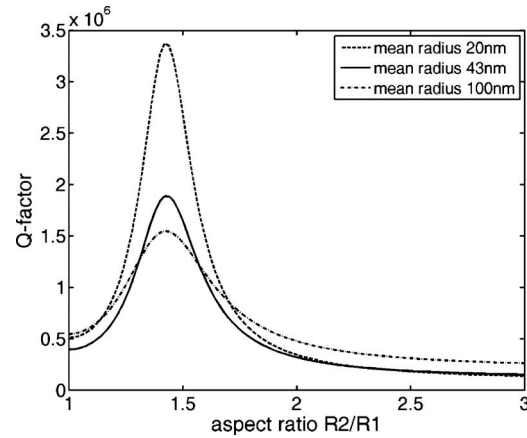


Fig. 13 Quality factor as a function of geometric aspect ratio in the contour-mode vibration of elliptical plate resonators

and may become dominant, therefore significantly reduce the Q value of the leading mode.

4 Conclusions

The energy dissipation related to thermoelastic damping has been studied for the contour-mode vibrations of rings, disks, and elliptical plates on various size scales. The key contributions of this research are (1) extension of the Fourier reduction method to the contour-mode vibrations of axisymmetric resonators, (2) application of the higher-order elements for improving numerical efficiency, and (3) quantitative investigation of thermoelastic damping in elliptical plates.

Customized finite element codes written on the MATLAB platform have been developed to solve the governing thermoelastic

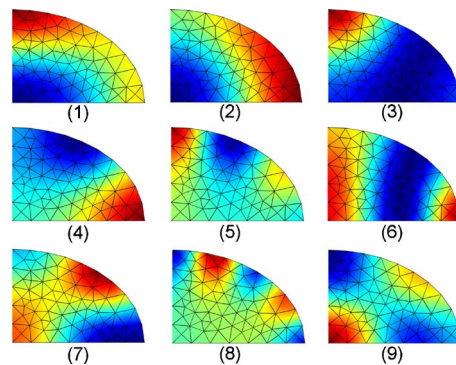


Fig. 14 Dominant mode patterns in the contour-mode vibration of elliptical plate resonator of aspect ratio 1.42

Table 3 Dominant modes of polysilicon elliptical resonator of mean radius 43 nm and aspect ratio 1.42

Mode No.	Frequency (MHz)	Q value
1	4.375×10^4	1.885×10^6
2	6.460×10^4	2.499×10^4
3	8.233×10^4	2.677×10^4
4	9.305×10^4	3.149×10^4
5	1.240×10^5	4.215×10^4
6	1.384×10^5	1.145×10^4
7	1.415×10^5	2.106×10^4
8	1.623×10^5	6.078×10^4
9	1.696×10^5	2.563×10^4

and dynamic matrix equations. The computational results on some limiting cases are compared to the analytical results found in literature. It has been found that using nonlinear elements can significantly improve the numerical accuracy. The application of the Fourier reduction scheme has greatly simplified the circular disk and ring models. With only three nodes in the radial direction, the nonlinear Fourier model yields a result very close to the exact solution. For elliptical plates, plane stress two-dimensional models have been developed to study their in-plane vibration modes. It is found that the plate aspect ratio has a relatively weak effect on the resonant frequency of the leading contour mode; however, its effect on the Q value is much more significant. In addition, the peak Q value occurs consistently in the vicinity of $\gamma=1.42$. Finally, this research has discovered and remedied some erroneous results related to thermoelastic damping in circular thin disks that were previously reported in literature.

Nomenclature

b	= exponential decaying rate
c_p	= specific heat capacity
D	= elasticity matrix
E	= Young's modulus
h	= beam thickness
k	= thermal conductivity
L	= beam length
m	= circumferential wave number (i.e., Fourier number)
\dot{q}	= volumetric heat generation rate
Q	= quality factor
r	= disk radius
t	= time
T	= temperature
T_0	= mean temperature
u	= displacement
W	= kinetic energy
ΔW	= kinetic energy loss per cycle
α	= thermal expansion coefficient
γ	= aspect ratio of elliptical plate
δ	= exponential damping factor
ε	= total strain
ε_t	= thermal strain
$\bar{\varepsilon}$	= dilatation strain
σ	= stress
ρ	= density
ν	= Poisson's ratio
ω	= natural frequency

ω_0 = undamped natural frequency
 Ψ = shape function

References

- [1] Evoy, S., Olkhovets, A., Sekaric, L., Parpia, J. M., Craighead, H. G., and Carr, D. W., 2000, "Temperature-Dependent Internal Friction in Silicon Nanoelectromechanical Systems," *Appl. Phys. Lett.*, **77**, pp. 2397–2399.
- [2] Houston, B. H., Photiadis, D. M., Marcus, M. H., Bucaro, J. A., Liu, X., and Vignola, J. F., 2002, "Thermoelastic Loss in Microscale Oscillators," *Appl. Phys. Lett.*, **80**, pp. 1300–1302.
- [3] Zener, C., 1937, "Internal Friction in Solids I: Theory of Internal Friction in Reeds," *Phys. Rev.*, **52**, pp. 230–235.
- [4] Lifshitz, R., and Roukes, M. L., 2000, "Thermoelastic Damping in Micro- and Nanomechanical Systems," *Phys. Rev. B*, **61**, pp. 5600–5609.
- [5] Nayfeh, A. H., and Younis, M. I., 2004, "Modeling and Simulations of Thermoelastic Damping in Microplates," *J. Micromech. Microeng.*, **14**, pp. 1711–1717.
- [6] Silver, M. J., and Peterson, L. D., 2005, "Predictive Elastothermodynamic Damping in Finite Element Models by Using a Perturbation Formulation," *AIAA J.*, **43**, pp. 2646–2653.
- [7] Kumar, S., and Haque, M. A., 2008, "Reduction of Thermo-Elastic Damping With a Secondary Elastic Field," *J. Sound Vib.*, **318**, pp. 423–427.
- [8] Wong, S. J., Fox, C. H. J., and McWilliam, S., 2006, "Thermoelastic Damping of the In-Plane Vibration of Thin Silicon Rings," *J. Sound Vib.*, **293**, pp. 266–285.
- [9] Sun, Y. X., and Tohmyoh, H., 2009, "Thermoelastic Damping of the Axisymmetric Vibration of Circular Plate Resonators," *J. Sound Vib.*, **319**, pp. 392–405.
- [10] Hao, Z. L., 2008, "Thermoelastic Damping in the Contour-Mode Vibrations of Micro- and Nano-Electromechanical Circular Thin-Plate Resonators," *J. Sound Vib.*, **313**, pp. 77–96.
- [11] Hao, Z., Pourkamali, S., and Ayazi, F., 2004, "VHF Single-Crystal Silicon Elliptic Bulk-Mode Capacitive Disk Resonators—Part I: Design and Modeling," *J. Microelectromech. Syst.*, **13**, pp. 1043–1053.
- [12] Pourkamali, S., Hao, Z., and Ayazi, F., 2004, "VHF Single Crystal Silicon Capacitive Elliptic Bulk-Mode Disk Resonators—Part II: Implementation and Characterization," *J. Microelectromech. Syst.*, **13**, pp. 1054–1062.
- [13] Tang, H. W., Yi, Y. B., and Matin, M. A., 2008, "Predictive Modeling of Thermoelastic Energy Dissipation in Tunable MEMS Mirrors" *J. Micro/Nanolith. MEMS MOEMS*, **7**, p. 023004.
- [14] Yi, Y. B., 2008, "Geometric Effects on Thermoelastic Damping in MEMS Resonators," *J. Sound Vib.*, **309**, pp. 588–599.
- [15] Yi, Y. B., and Matin, M. A., 2007, "Eigenvalue Solution of Thermoelastic Damping in Beam Resonators Using a Finite Element Analysis," *ASME J. Vib. Acoust.*, **129**, pp. 478–483.
- [16] Yi, Y. B., Rahafrooz, A., and Pourkamali, S., 2009, "Modeling and Testing of the Collective Effects of Thermoelastic and Fluid Damping on Silicon MEMS Resonators," *J. Micro/Nanolith. MEMS MOEMS*, **8**, p. 023010.
- [17] 2006, COMSOL MULTIPHYSICS 3.3 User's Manual, COMSOL, Inc., Los Angeles, CA.
- [18] Yi, Y.-B., Barber, J. R., and Zagrodzki, P., 2000, "Eigenvalue Solution of Thermoelastic Instability Problems Using Fourier Reduction," *Proc. R. Soc. London, Ser. A*, **456**, pp. 2799–2821.
- [19] Yi, Y. B., 2006, "Finite Element Analysis on Thermoelastodynamic Instabilities Involving Frictional Heating," *ASME J. Tribol.*, **128**, pp. 718–724.
- [20] Reddy, J. N., 2006, *An Introduction to the Finite Element Method*, 3rd ed., McGraw-Hill, New York.